J. Am. Soc. Mass Spectrom. (2015) 26:2105–2114
DOI: 10.1007/s13361-015-1226-7

RESEARCH ARTICLE

Differentiating Fragmentation Pathways of Cholesterol by Two-Dimensional Fourier Transform Ion Cyclotron Resonance Mass Spectrometry

Maria A. van Agthoven,[1] Mark P. Barrow,[1] Lionel Chiron,[2] Marie-Aude Coutouly,[2] David Kilgour,[3] Christopher A. Wootton,[1] Juan Wei,[1] Andrew Soulby,[1] Marc-André Delsuc,[2,4] Christian Rolando,[5] Peter B. O'Connor[1]

[1]Department of Chemistry, University of Warwick, Coventry, CV4 7AL, UK
[2]NMRTEC, Bld. Sébastien Brandt, Bioparc - Bat. B, 67400, Illkirch-Graffenstaden, France
[3]School of Pharmacy, University of Maryland, Baltimore, MD 21201, USA
[4]Institut de Génétique et de Biologie Moléculaire et Cellulaire, INSERM, U596; CNRS, UMR7104, Université de Strasbourg, 1 rue Laurent Fries, 67404, Illkirch-Graffenstaden, France
[5]Miniaturisation pour la Synthèse, l'Analyse & la Protéomique (MSAP), USR CNRS 3290, and Protéomique, Modifications Post-traductionnelles et Glycobiologie, IFR 147 and Institut Eugène-Michel Chevreul, FR CNRS 2638, Université de Lille 1 Sciences et Technologies, 59655, Villeneuve d'Ascq Cedex, France

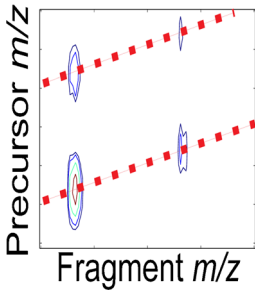

Abstract. Two-dimensional Fourier transform ion cyclotron resonance mass spectrometry is a data-independent analytical method that records the fragmentation patterns of all the compounds in a sample. This study shows the implementation of atmospheric pressure photoionization with two-dimensional (2D) Fourier transform ion cyclotron resonance mass spectrometry. In the resulting 2D mass spectrum, the fragmentation patterns of the radical and protonated species from cholesterol are differentiated. This study shows the use of fragment ion lines, precursor ion lines, and neutral loss lines in the 2D mass spectrum to determine fragmentation mechanisms of known compounds and to gain information on unknown ion species in the spectrum. In concert with high resolution mass spectrometry, 2D Fourier transform ion cyclotron resonance mass spectrometry can be a useful tool for the structural analysis of small molecules.

Keywords: FT-ICR MS, Fourier transform ion cyclotron resonance mass spectrometry, Two-dimensional, IRMPD, Infrared multiphoton dissociation, APPI, Atmospheric pressure photoionization, Cholesterol

Received: 8 December 2014/Revised: 18 May 2015/Accepted: 20 May 2015/Published Online: 17 July 2015

Introduction

The principles of Fourier-transform ion cyclotron resonance mass spectrometry (FT-ICR MS) are based on the cyclotron motion of ions in a homogeneous magnetic field [1, 2]. Ions are trapped in an ultra-high-vacuum ICR cell with two axial trapping electrodes, two excitation electrodes on which a swept-frequency rf potential is applied to excite the ions coherently to an appropriate orbital radius, and two detection electrodes are used to measure the image current generated by the ion packet's motion. The frequencies of the image current reflect the frequencies of the ion motion, which is then calibrated to yield the mass-to-charge ratio (m/z) of the ions inside the ICR cell. Because FT-ICR MS is based on a time measurement and because an ion's frequency is independent of kinetic energy, this technique provides the highest resolving power and mass accuracy currently available [3].

As a result of its reliance on high magnetic fields and Fourier transformation, FT-ICR MS has parallels to nuclear magnetic

Associated Content Table containing the m/z of the most abundant ion species detected in the mass spectrum presented in Figure 1a and chemical formulae attributions.

Tables containing the m/z of all the ion species detected in the mass spectra presented in Figure 1b and 1c, chemical formulae attribution and fragmentation pathways.

Electronic supplementary material The online version of this article (doi:10.1007/s13361-015-1226-7) contains supplementary material, which is available to authorized users.

Correspondence to: Peter O'Connor; *e-mail:* p.oconnor@warwick.ac.uk

resonance (NMR) spectroscopy. However, unlike NMR spectroscopy, the potential of multidimensional FT-ICR MS remains largely unexplored. First introduced by Pfaendler et al. in 1987 [4], two-dimensional FT-ICR MS (2D FT-ICR MS) relies on ion de-excitation by phase reversal of the excitation voltage [5]. The basic pulse sequence for 2D FT-ICR MS, shown in Scheme 1, has two encoding pulses separated by a regularly incremented delay t_1. At the end of the second encoding pulse, the precursor ion's cyclotron radius is modulated according to t_1 and its cyclotron frequency [6]. During the subsequent fragmentation period, the precursor ion fragmentation efficiency as well as the fragment ion abundance depends on the radius of the precursor ion at the end of the encoding sequence (see Scheme 1). After fragmentation, all ions are excited to high radius and detected. The resulting dataset can be Fourier transformed along the detection (t_2) and the delay (t_1) dimensions.

As the fragmentation efficiency of the precursor ions and the abundance of the fragment ions are both modulated according to the cyclotron frequency of the precursor, the resulting 2D map in the *m/z* domain, or 2D mass spectrum, shows peaks for each dissociation in which the first coordinate (chosen by convention to be the horizontal axis) is the fragment *m/z*, and the second coordinate (by convention, the vertical axis) is the precursor *m/z*. Scheme 2 shows a diagram of a 2D mass spectrum and how to interpret it. Significant lines in a 2D mass spectrum include the autocorrelation line, which shows the *m/z* of all the precursors, horizontal fragment ion scans, which show the fragmentation pattern of a given precursor ion, and vertical scans, which show all the precursors of a given fragment ion [7].

2D FT-ICR MS was first used in conjunction with ion-molecule reactions [8] and infrared multiphoton dissociation (IRMPD) [9]. Due to limitations in computer hardware, however, 2D FT-ICR MS was not developed much further, despite Ross et al. developing an alternative ion radius modulation method, stored waveform ion radius modulation (SWIM) [10, 11], which was also used by van der Rest and Marshall to study noise phenomena in 2D mass spectra [12]. In 2010, 2D FT-ICR MS using the original pulse sequence was implemented again using IRMPD [13] and electron capture dissociation (ECD) [14] for peptides from a nanoelectrospray ion source. Advances in data processing and denoising algorithms were made [15, 16], and the pulse sequence was optimized in order to maximize signal-to-noise ratios [17].

This study shows the first coupling of 2D FT-ICR MS with an atmospheric pressure photoionization (APPI) [18, 19] source, which, as a continuous ion source for both polar and nonpolar compounds [20, 21], is a natural expansion for 2D

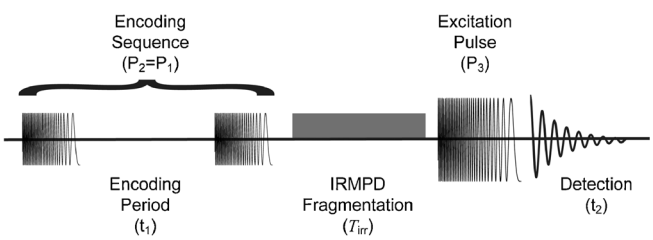

Scheme 1. Pulse sequence of the 2D FT-ICR MS experiment

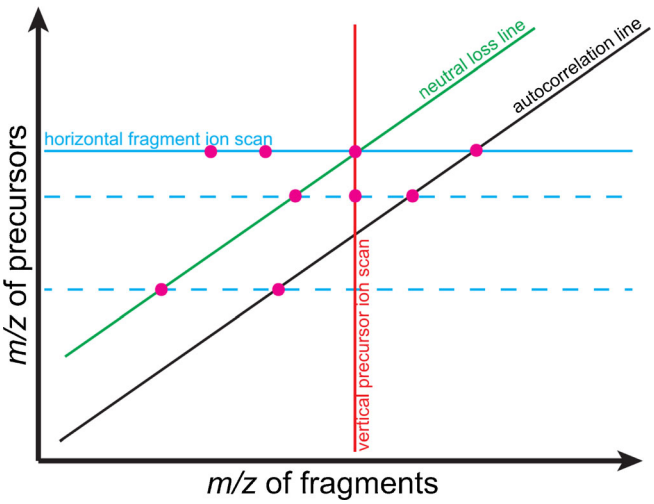

Scheme 2. Interpretation of a 2D mass spectrum

FT-ICR MS. APPI can produce both radical and protonated species, and limited oxidation and fragmentation can occur [22]. Combined with IRMPD as a fragmentation mode, 2D APPI FT-ICR MS allows the differentiation of the fragmentation pathways for both radical and protonated species within the same experiment.

Cholesterol is a compound with well-known fragmentation patterns that allows the illustration of the use of 2D FT-ICR MS for small molecules [23]. In concert with high resolution FT-ICR MS to measure the exact *m/z* of both precursor and fragment ions, 2D FT-ICR MS showed the fragmentation pathways of cholesterol and structural information of the front-end fragment ions or oxidized ions [22] as well as contaminants in the sample.

Experimental

A solution of cholesterol (Sigma Aldrich, Dorset, UK) was prepared at 100 pmol/μL in acetonitrile (VWR International, Ltd., Lutterworth, United Kingdom) and water (75:25). The water was purified using a Direct-Q 3 Ultrapure Water System (Millipore, Nottingham, United Kingdom).

The sample was ionized using an APPI II ion source with a krypton lamp (Bruker Daltonik GmbH, Bremen, Germany). The syringe flow rate was 600 μL/h, the capillary voltage was +1500 V, the spray shield offset voltage was –500 V, the nebulizer gas (N_2) pressure was 0.8 bar at 350°C, and the heated drying gas (N_2) flow pressure was 0.8 bar at 250°C. All experiments were performed on a 12 T solariX Fourier transform ion cyclotron resonance mass spectrometer (Bruker Daltonik GmbH, Bremen, Germany). Ions were transferred through two electronic ion funnels and a quadrupole before being accumulated in a hexapole-based collision cell for 0.1 s. A hexapole ion guide (4 MHz frequency at 350 V_{pp} with –10 V on the entrance lens and –8.0 V on the analyzer entrance lens before trapping) was used to transfer the ions to the infinity cell [24]. Ions were then transferred to the infinity cell through a

focusing ion guide and a hexapole during a 1.0 ms transfer period. The Sidekick voltage was kept at –10 V and the Sidekick offset was set to –1.0 V. Both the front and the back plate trapping potentials were set to 0.6 V.

Control Mass Spectra and Product-Ion Spectra

The control mass spectrum was measured with 4 Mword (16 bit) transients lasting 1.6777 s over *m/z* 147.4–500 (368.5–1250 kHz frequency range), with a pulse at 14% excitation power (65 V_{pp} amplitude) and 20 μs per frequency in 1411 steps of 624.78 Hz frequency decrement. The control product-ion spectra were measured with similar parameters, but with a *m/z* 36.9–500 mass range (i.e., a 5000–368.5 kHz frequency range). Each spectrum resulted from the accumulation of 20 scans.

For product-ion spectra, ion isolation was performed using the quadrupole with an *m/z* 2.5 window. IRMPD was performed using a Synrad 48-2 CO_2 laser (25 W) with a 10.6 μm wavelength and a 0.1 s irradiation length at 50% power (Synrad, Mukilteo, WA, USA).

The mass spectrum was phase-corrected using the Autophaser 6.0 phase correction software [25–32]. All one-dimensional (1D) spectra were first externally calibrated in the solariXControl software (Bruker Daltonics, Billerica, MA, USA) using Agilent ESI-L Low Concentration Tuning Mix (Agilent Technologies, Stockport, United Kingdom), and then internally calibrated against the theoretical *m/z* values of the ions generated by cholesterol using the quadratic calibration function within Data Analysis 4.0 (Bruker Daltonik GmbH, Bremen, Germany) [33].

2D Mass Spectrum

The pulse sequence of the 2D FT-ICR MS experiment is presented in Scheme 1. The two encoding pulses P_1 and P_2 were identical with a 15% excitation power (70 V_{pp} amplitude) and 0.4 μs per frequency over a 368.5–5000 kHz frequency range (*m/z* 36.9–500 mass range). The encoding period t_1 started at 0.5 μs with 2048 increments of 0.5 μs each (0.5–1024.5 μs). As a result, the Nyquist frequency in the precursor ion dimension (ω_1) was 1000 kHz, corresponding to a minimum *m/z* ratio of 184.27 for a precursor ion in the 2D mass spectrum. The fragmentation period was 0.1 s at 50% power of the IRMPD laser (12.5 W). Each transient was recorded with 128 k datapoints over an *m/z* 36.9–500 mass range (i.e., a 5000–368.5 kHz frequency range), with an excitation pulse P_3 at 14% excitation power (65 V_{pp} amplitude) and 20 μs per frequency. In total, 2048 times 128 k datapoints were acquired over 17 min. Each transient lasted 0.0262 s.

Data processing was performed using NPKV2 (NMR Processing Kernel), which was developed independently by the University of Strasbourg and NMRTEC (Illkirch-Graffenstaden, France) in 64-bit Python programming language using the commercial platform distributed by Anaconda Continuum Analytics (Austin, TX, USA) [34]. NPKV2 is freely available from the authors. Processed data files were saved using the HDF5 file format. In the precursor ion dimension (ω_1), the signals were digitally demodulated by applying a time-dependent phase rotation as a function of t_1 before Fourier transformation. The results are plotted in magnitude mode. All frequencies were converted into *m/z* using Francl's equation, with parameters that were determined using external calibration for a mass spectrum because of computational ease [35, 36]. The same calibration parameters were used in the ω_1 dimension and the ω_2 dimension.

Results and Discussion

Figure 1a shows the FT-ICR mass spectrum of cholesterol ionized using APPI. The mass spectrum shows the molecular ion from cholesterol (see Scheme 3), but only as a radical cation. Peaks corresponding to single or multiple in-source dehydrogenations of cholesterol were observed, as well as ion species resulting from water loss by cholesterol, both in odd-electron and even-electron form (protonated cholesterol has been almost entirely fragmented in the ion source). The sample also contains a number of cholesterol oxidation products.

With phase correction, the resolving power of the peaks is approximately 600,000 (full width at half maximum [FWHM]) at *m/z* 400. Internal calibration of the mass spectrum using the known peaks of cholesterol enabled the assignment of the molecular composition of the unknown peaks in the mass spectrum (results for the 100 most abundant peaks in the Supplementary Materials, Table 1) [3]. As a result, the chemical formulas and the abundance of the compounds in the mass spectrum, as well as their in-source fragment ions, were determined. The most abundant species is cholesterol (69%), but $C_cH_hN_5O$, $C_cH_hN_2O$, $C_cH_hN_2$, $C_cH_hNO_5$, $C_cH_hNO_3$, C_cH_hNO, C_cH_hN, $C_cH_hO_6$, $C_cH_hO_4$, $C_cH_hO_3$, $C_cH_hO_2$, C_cH_hO compounds and hydrocarbons were also found (with c between 16 and 31, h between 31 and 51).

Figure 1b and c show the IRMPD fragmentation patterns of the $M^{+\bullet}$ ion at *m/z* 386 and the $[M+H-H_2O]^+$ ion at *m/z* 369. All the peaks are identified in Tables 2 and 3 in the Supplementary Materials. The peaks in Figure 1b correspond to the fragments of cholesterol as identified by Wyllie et al. [23]. The fragmentation pattern in Figure 1c from the *m/z* 369 ion (resulting from the in-source loss of water from cholesterol) shows groups of hydrocarbon fragments with increasing carbon numbers with various double bond equivalents (DBE).

For both product-ion spectra, the quadrupole isolation window was set at *m/z* 2.5 in order to minimize ion loss, which affects IRMPD sensitivity. For the product-ion spectrum of the *m/z* 386 ion, there are several possible precursor ions in this window: $[M+H-H_2]^+$, $[M-H_2]^{+\bullet}$, and $M^{+\bullet}$. For the product-ion spectrum of the *m/z* 369 ion, they are: $[M-H_2O]^{+\bullet}$, $[M+H-H_2O]^+$, $[M+H-H_2O-H_2]^+$ or $[M-H_2-CH_3]^+$. As a result, determining whether an even-electron fragment ion results from the loss of a neutral radical by a radical ion or from the loss of an even-electron neutral by an even-electron ion is not

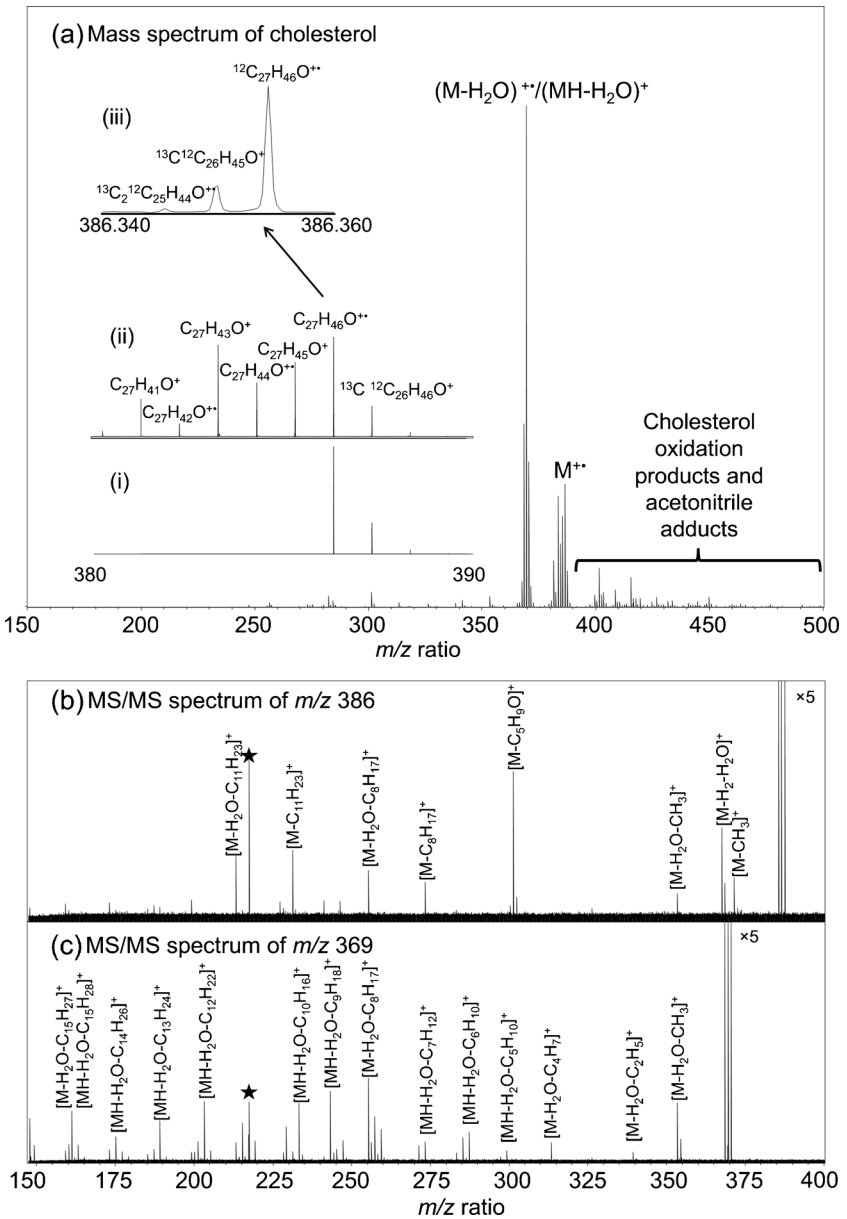

Figure 1. **(a)** APPI FT-ICR mass spectrum of cholesterol. (i) Theoretical isotopic distribution of the $M^{\bullet+}$ ion of cholesterol. (ii) Zoom-in on the ions generated from cholesterol and their elemental formulae. (iii) Isotopic fine structure of the peak at *m/z* 386.35. **(b)** IRMPD product-ion FT-ICR mass spectra of the quadrupole-isolated ions of **(a)** *m/z* 386 ($M^{+\bullet}$) and **(b)** *m/z* 369 ($[MH - H_2O]^+$) of cholesterol. Peak marked with a star: artifact peak showing at *m/z* 217.3958

possible with quadrupole-isolation MS/MS. Using this experimental setup, determining whether two peaks separated by the mass of H_2 are generated from two precursors that are differentiated by a double bond, or if the two fragments are generated by the same precursor with the same fragmentation mechanism, followed by dehydrogenation, is equally impossible with quadrupole-isolation MS/MS.

With adequate automation and visualization software, MS/MS can be used to generate 2D mass spectra in a data-independent fashion. A very similar method is used in precursor acquisition independent from ion count (PAcIFIC) [37] in conjunction with liquid chromatography for proteomics analysis. For comparison with the present study, if using only MS/MS, with a precursor mass range of *m/z* 184.27–500 and a precursor resolving power of 1 Da, 315 product-ion spectra would need to be recorded in order to cover the same precursor mass range with the same resolution. Several tens of scans would also need to be accumulated in order to obtain a signal-to-noise ratio that is comparable to the signal-of-noise ratio of the 2D mass spectrum. The resulting experiment would consume both more time and more sample than 2D FT-ICR MS. Furthermore, with quadrupole isolation, increasing the resolution in precursor selection goes hand in hand with a decrease in signal intensity, which is not an issue in the 2D FT-ICR experiment [38].

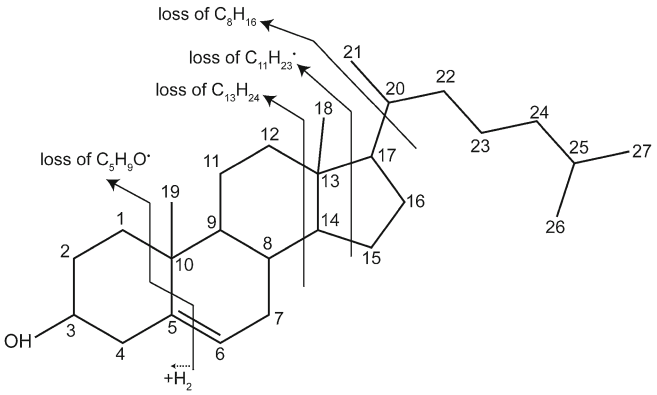

Scheme 3. Structure of cholesterol and some observed cleavages

Other isolation methods, such as SWIFT [39, 40] or CHEF [39, 41–45], are available for high-resolution isolation windows within the ICR cell. Other ion trapping devices, like linear or quadrupolar ion traps [46], can select ions with a narrow isolation window (1 Da or better) using tailored waveforms. However, because such an isolation in a linear/quadrupole ion trap would involve increasing the selected ions' kinetic energy in a buffer gas, they present the probability of uncontrolled fragmentation because of the isolation that may be confused for products of the desired fragmentation mode (no fragmentation is observed using SWIFT/CHEF isolations in an ICR cell).

In 2D FT-ICR MS, correlation between precursor and fragment ions is achieved through ion radius modulation of the precursor ions during the encoding sequence (see Scheme 1) according to the cyclotron frequency of the precursor ions [7]. Unlike standard MS/MS, the fragmentation patterns in 2D FT-ICR MS are measured in a parallel manner. Because 2D FT-ICR MS experiments are Fourier transform-based temporal measurements, the resolving power depends upon the frequency and the acquisition time, which is, in turn, dependent upon the sampling frequency and the dataset size at low enough pressure. As a result, resolving the correlation between precursor and fragment ions without losing signal intensity is possible as long as the number of data points in the dataset is sufficient. Furthermore, because all ions created before the start of the pulse sequence in the ICR cell have the same behavior (i.e., they are trapped at the center of the ICR cell), distinguishing fragments generated in the ion source and in the ICR cell in the 2D mass spectrum is straightforward: ions created in the ion source show a peak on the autocorrelation line, whereas ions created in the ICR cell during the fragmentation period do not (see Scheme 1). As a result, 2D mass spectrometry can easily distinguish between fragments produced in the front end of the FT-ICR instrument and those produced within the ICR cell without the need for complex MS/MS experiments involving tailored waveforms in the cell for high resolution isolation.

Figure 2a shows the 2D mass spectrum of cholesterol with the same fragmentation conditions as the standard product-ion spectra in Figure 1b and c. Figures 2b to i are extracted spectra from Figure 2a. Each peak in Figure 2a corresponds to a dissociation occurring during the fragmentation period in the pulse sequence (see Scheme 1): the vertical coordinate of the peak is the *m/z* ratio of the precursor ion, and the horizontal coordinate of the peak is the *m/z* ratio of the fragment ion. Precursor ion peaks have the same coordinate on both axes and, therefore, are situated on the autocorrelation line. All the fragment ions of a given precursor can be viewed horizontally along a fragment ion scan, and all the precursors of a given fragment can be viewed vertically along a precursor ion scan, as shown in Figure 2d. Neutral loss scans are parallel to the autocorrelation line and are shifted by the mass of the neutral species lost. As a result, one experiment yields precursor ion scans, fragment ion scans, and neutral loss scans. In Figure 2a, we can see neutral loss lines for loss of H_2O and loss of $CH_3^{\bullet}$, with peaks along these lines corresponding to dissociations originating from cholesterol and from other ion species.

The size of the dataset is 2048 scans (i.e., increments of t_1) of 128 k data point transients. The experiment lasted for 17 minutes, and 170 μL of sample was consumed by direct infusion. The limit on the size of the dataset was imposed by the sample flow rate and the syringe size. Owing to those limitations for this ion source, resolving powers are limited to 10,000 in the horizontal direction for fragment ions and of 300 in the vertical direction for precursor ions at *m/z* 386. This resolving power was sufficient to separate precursors vertically with a 1 Da mass difference, allowing the assignment of the fragmentation patterns of odd-electron and even-electron ions. In the rest of this study, mass-to-charge values were measured in the horizontal dimension with 0.01 Da precision, and *m/z* measured in the vertical dimension with 1 Da precision to be consistent with the resolution of the peaks in either dimension.

Despite the optimization of the pulse sequence [17], vertical lines are visible along the most intense peaks corresponding to scintillation noise and curves corresponding to harmonics. However, the signal-to-noise ratio of the data was sufficient and the precursors were simple enough that denoising was not deemed necessary to interpret the 2D mass spectrum [16]. Because all precursors are singly charged, it is clear that the area of the 2D mass spectrum on the right side of the autocorrelation line (i.e., higher *m/z*) does not show real fragmentation peaks (as this would require the fragment ions to be higher in mass than the precursor ions). However, care must be taken to avoid scintillation noise.

Figure 2b and c show two expanded regions of the 2D mass spectrum. Figure 2b shows a cluster of dissociation peaks resulting in fragments ions between *m/z* 213–220 horizontally. The peaks are observed at *m/z* 368 for the $[M - H_2O]^{+\bullet}$ ion, *m/z* 369 for the $[M+H - H_2O]^+$ ion, and *m/z* 386 for the $M^{+\bullet}$ ion vertically, allowing correlation with the precursors of each fragment. Similar interpretations can be made for all the other regions of the 2D mass spectrum.

The fragment peaks originating from the *m/z* 368 $[M - H_2O]^{+\bullet}$ ion and the *m/z* 369 $[M+H - H_2O]^+$ ion can be very clearly distinguished. The peaks at *m/z* 213.1638, *m/z* 214.1716, *m/z* 215.1794, *m/z* 216.1873, *m/z* 217.1951, and *m/z* 219.2107 can all be found in the product-ion spectrum of *m/z* 369 presented in Figure 1c, and whether their precursor is

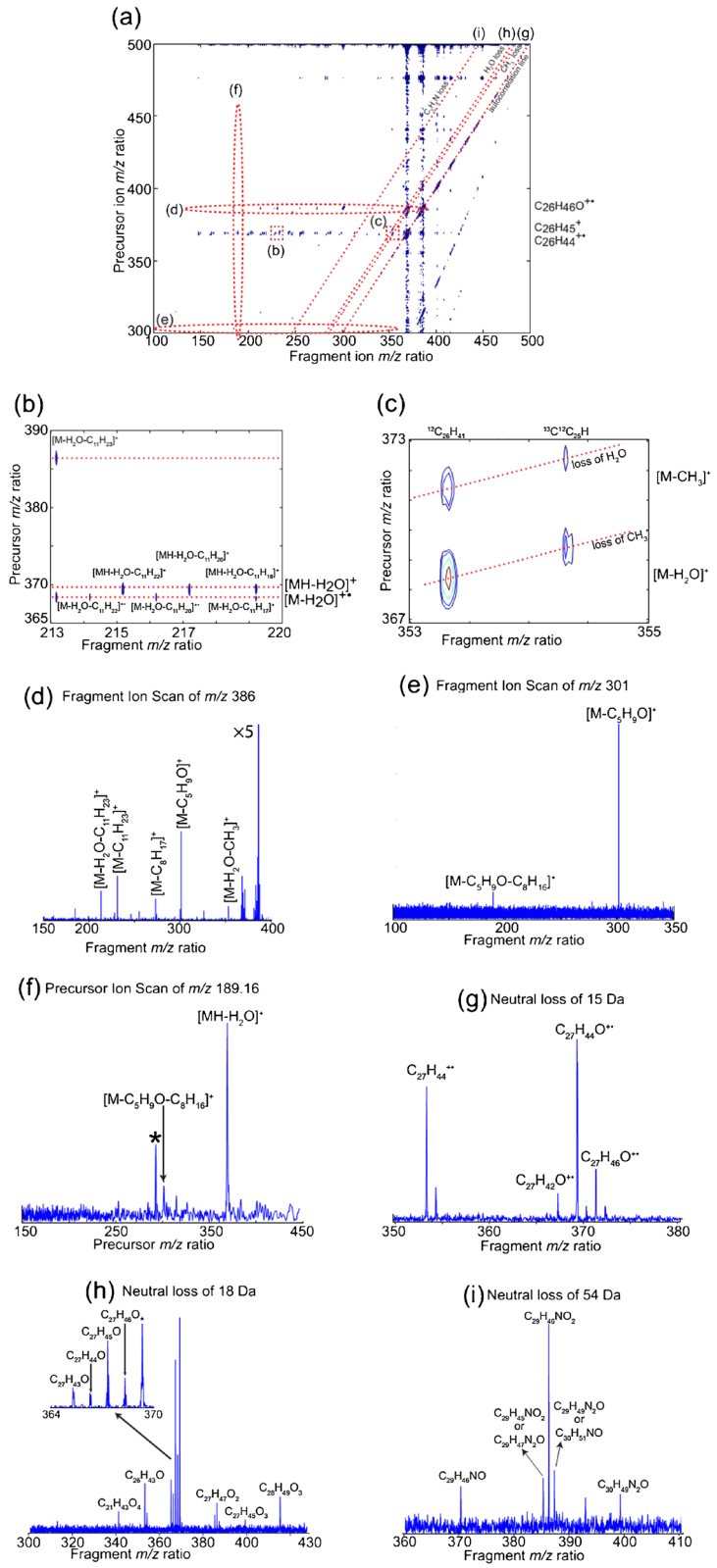

Figure 2. **(a)** APPI 2D IRMPD FT-ICR mass spectrum of cholesterol. Expanded regions: **(b)** *m/z* 213–220 horizontally and *m/z* 365–390 vertically, and **(c)** *m/z* 353–355 horizontally and *m/z* 367-373 vertically. Profiles: **(d)** Fragment ion scan of *m/z* 386. **(e)** Fragment ion scan of *m/z* 301. **(f)** Precursor ion scan of *m/z* 189.16. * Harmonic peak from *m/z* 369 [17]. **(g)** Neutral loss scan for a loss of 15 Da. **(h)** Neutral loss scan for a loss of 18 Da. (i) Neutral loss scan for a loss of 54 Da. *^{13}C isotope peak distorted by scintillation noise from the precursor peak of *m/z* 369

$[M - H_2O]^{+\bullet}$, $[M+H - H_2O]^+$, or both, can easily be determined in the 2D mass spectrum.

The fragment ion at *m/z* 213.16, assigned to $C_{16}H_{21}^+$ in both high-resolution 1D product-ion spectra (see Figure 1b and c), shows two peaks at *m/z* 368 and 386 on the vertical axis, which indicates that its two precursors are $M^{+\bullet}$ and $[M - H_2O]^{+\bullet}$, proving that loss of H_2O and loss of $C_{11}H_{23}^{\bullet}$ (155.18 Da, change in double bond equivalent of 0.5) occur sequentially. The peak for $C_{16}H_{23}O^+$, at *m/z* 231.17, is also present in both the product-ion spectrum of *m/z* 386 and the 2D mass spectrum as a fragment of $M^{+\bullet}$ alone (see Tables 2 and 3 in the Supplementary Materials). This suggests that the loss of $C_{11}H_{23}^{\bullet}$ occurs along C_{13}-C_{17} and C_{14}-C_{15} (see Scheme 3).

Unlike the fragment ion at *m/z* 213.16 ($C_{16}H_{21}^+$), the fragment ion at *m/z* 214.17 ($C_{16}H_{22}^+$) only arises from $[M - H_2O]^{+\bullet}$ (loss of $C_{11}H_{22}$). $[M - C_{11}H_{22}]^{+\bullet}$ is present at *m/z* 232.18 ($C_{16}H_{24}O^+$) in the product-ion spectrum of *m/z* 386, but in very low abundance (see Table 2 in the Supplementary Materials), and is below detection level in the 2D mass spectrum.

The fragment ion at *m/z* 215.18 ($C_{16}H_{23}^+$) arises from the loss of $C_{11}H_{22}$ from $[M+H - H_2O]^+$. Since the fragment ion at *m/z* 214.17 ($C_{16}H_{22}^+$) also originates from loss of $C_{11}H_{22}$ from $[M - H_2O]^{+\bullet}$, either the loss of $C_{11}H_{22}$ can happen via two different fragmentation mechanisms, or this loss does not involve either the proton or the radical. Similarly, the fragment ions at *m/z* 216.19 ($C_{16}H_{24}^+$) and *m/z* 217.20 ($C_{16}H_{27}^+$) originate from the loss of $C_{11}H_{20}$ from $[M - H_2O]^{+\bullet}$ and $[M+H - H_2O]^+$, respectively. Differentiating the fragmentation pattern of $[M+H - H_2O]^+$ from the isotopic patterns of $[M - H_2O]^{+\bullet}$ is possible because of the intensity of the peaks: the ion species were differentiated by matching the isotopic pattern of the $[M - H_2O]^{+\bullet}$ and $[M+H - H_2O]^+$ precursor species showing the overlap of the ^{13}C peak of $[M - H_2O]^{+\bullet}$ and $[M+H - H_2O]^+$. The two isotopic distributions can be resolved in the 1D product-ion spectra.

The fragment ion at *m/z* 219.21 originates both from $[M - H_2O]^{+\bullet}$ and $[M+H - H_2O]^+$ and results from the loss of $C_{11}H_{17}^{\bullet}$ and $C_{11}H_{18}$, respectively. The two mechanisms resulting in the ion at *m/z* 219.21 are different, but any conclusions as to its chemical structure require an additional fragmentation stage.

No fragment peaks at vertical *m/z* 366 (corresponding to $C_{27}H_{42}^{+\bullet}$), *m/z* 367 (corresponding to $C_{27}H_{43}^+$), *m/z* 384 (corresponding to $C_{27}H_{44}O^{+\bullet}$), or *m/z* 385 (corresponding to $C_{27}H_{45}O^+$) are observed in Figure 2b. As a result, the dehydrogenations occurring in the front-end of the mass spectrometer apparently inhibit the fragmentation channels leading to the loss of $C_{11}H_{17}^{\bullet}$, $C_{11}H_{18}$, $C_{11}H_{20}$, $C_{11}H_{22}$, and $C_{11}H_{23}^{\bullet}$.

Finally, the artifact peak at *m/z* 217.39 is present in both product-ion spectra shown in Figure 1b and c and is absent in Figure 2b. Owing to the radial modulation of the precursor ions in the pulse sequence for 2D FT-ICR MS, artifacts do not show peaks in the horizontal fragment scan as actual fragments would do [17]. As a result, *m/z* 217.39 can be ruled out as a fragment ion, and as its frequency is approximately 850 kHz, can be assigned to rf interference from the multipoles.

Figure 2c shows a cluster of fragments between *m/z* 353 and 355 horizontally and *m/z* between 367 and 373 vertically, corresponding to the fragmentation pathways leading to $C_{26}H_{41}^+$. This fragment ion, at horizontal *m/z* 353.32, has two peaks: one peak at vertical *m/z* 368, corresponding to precursor ion $[M - H_2O]^{+\bullet}$, and one peak at vertical *m/z* 371, corresponding to precursor ion $[M - CH_3]^{+\bullet}$. The fact that in-source fragments are on the autocorrelation line in the 2D mass spectrum shows that the ion at *m/z* 353.32 results from loss of H_2O in the front-end of the instrument followed by loss of $CH_3^{\bullet}$ in the ICR cell or from loss of $CH_3^{\bullet}$ in the APPI source followed by loss of H_2O in the ICR cell. The 2D mass spectrum also shows a peak at vertical *m/z* 386 and horizontal *m/z* 353.32, showing that $M^{+\bullet}$ also loses both H_2O and $CH_3^{\bullet}$ in the ICR cell (see Figure 2a).

Figure 2c also shows the isotopic pattern of the $C_{26}H_{41}^+$ (*m/z* 353.32) fragment ion along the neutral loss lines corresponding to the dissociations that lead to it. In 2D mass spectra, the isotopic distribution of a fragment ion can always be found along the neutral loss line of the fragment [14]. In this case, the isotopic pattern of Figure 2c can be differentiated from the $[M -H_2O]^{+\bullet}$/ $[M+H - H_2O]^+$ precursor states in Figure 2c by the relative intensities of the peaks, despite the resolving power in either horizontal or vertical dimension being too low to separate the two (the minimum necessary resolving power in standard MS would be 80,000, FWHM).

Figure 2d shows the fragment ion scan of *m/z* 386, which corresponds to the fragmentation pattern of $M^{+\bullet}$. This fragment ion scan is equivalent to the product-ion spectrum of *m/z* 386 shown in Figure 1b, and indeed the two mass spectra show many of the same cholesterol fragment peaks.

Figure 2e shows the fragmentation pattern of *m/z* 301, which is an in-source fragment of cholesterol that has been identified as $[M - C_5H_9O]^+$ in the mass spectrum (see Figure 1a and Table 1 in the Supplementary Materials). The product-ion spectra (see Figure 1b and c) and the 2D mass spectrum (see Figure 2a) show that the ion at *m/z* 301.19 is a fragment of $M^{+\bullet}$, but not of MH^+, $[M - H_2O]^{+\bullet}$, or $[M+H - H_2O]^+$. Budzikiewicz and Ockels [47] and Wyllie et al. [23] have shown independently that the cleavage resulting in $[M - C_5H_9O]^+$ includes breaking the double bond between C_5 and C_6 (see Scheme 3), which suggests that for this fragment, ionization occurs by taking an electron from the π bond, unlike $M^{+\bullet}$ ions losing a water molecule, in which ionization occurs by taking an electron from one of the free lone pairs of the oxygen.

As the ion at *m/z* 301.19 ($C_{22}H_{36}^+$ or $[M - C_5H_9O]^+$) corresponds to an in-source fragment of cholesterol (see Table 1 in the Supplementary Materials), the IRMPD MS^3 fragmentation can be seen in the 2D mass spectrum. The fragment ion scan in Figure 2e shows that $C_{22}H_{36}^+$ dissociates into an ion at *m/z* 189.16 ($C_{14}H_{21}^+$) by losing C_8H_{16}. Budzikiewicz et al. [47] showed that androst-5-en-3β-ol, which has the same structure as cholesterol without the alkyl chain on C_{17}, also fragments into an ion at *m/z* 189.16 (see Scheme 3). Therefore, $[M - C_5H_9O]^+$ likely fragments into $C_{14}H_{21}^+$ by first losing part of the alkyl chain.

Figure 2f shows the precursor ion scan of the ion at *m/z* 189.16, which is shown to arise from an ion at *m/z* 301. The other precursor (*m/z* 369) corresponds to $[M+H - H_2O]^+$ of cholesterol and loses $C_{13}H_{24}$ to dissociate into *m/z* 189.16. According to Rossmann et al. [48], the cleavage may occur along C_{12}-C_{13} and C_8-C_{14} (see Scheme 3), which could mean that *m/z* 189.16 could be derived from isomers resulting from two different fragmentation pathways.

In Figure 1, the high resolution and mass accuracy of the analyzer allows the assignment the molecular formulae of the contaminants (see Table 1 in the Supplementary Materials). The mass spectrum alone without fragmentation, however, yields little information on the chemical structure of the contaminants. One-dimensional control product-ion spectra were not recorded for the contaminant peaks, but the data-independent nature of 2D FT-ICR MS allows the visualization of the fragmentation patterns of the contaminant peaks. Identifying the neutral losses in the 2D mass spectrum gives information on ion species whose structures are a priori unknown.

Neutral loss scans can be viewed on lines following Eq. 1 [14]:

$$(m/z)_{precursor} = (m/z)_{fragment} + m_{neutral} \quad (1)$$

Figure 2g, h, and i show the neutral loss scans of $CH_3^{\bullet}$ (Figure 2g), one water molecule (Figure 2h), and C_3H_4N (Figure 2i). The *m/z* axis corresponds to the fragment ion peaks, but the *m/z* of the precursors can easily be calculated using Eq. 1. Loss of $CH_3^{\bullet}$ occurs only from the radical cation, which is reflected in Figure 2g: the species losing $CH_3^{\bullet}$ are $C_{27}H_{44}^{+\bullet}$, $C_{27}H_{42}O^{+\bullet}$, $C_{27}H44O^{+\bullet}$, and $C_{27}H_{46}O^{+\bullet}$. Loss of a water molecule indicates that there is an alcohol group in the precursor.

In cases where a fragment ion is also present as an abundant precursor on the autocorrelation line (i.e., front-end fragment ion species, for example), scintillation noise can cause additional peaks in the neutral loss lines that can overlap with the fragment ion peak [15]. Checking whether a peak in the neutral loss scan represents a fragmentation or scintillation noise is important to avoid faulty interpretations.

In Figure 2h, the resolution at *m/z* 369 is 10,000 (FWHM of 0.04 Da). This value is both the resolution in the vertical precursor dimension and the resolution in the horizontal fragment dimension. Because the signal in the vertical precursor dimension (2048 data points) and in the horizontal fragment dimension (131,072 data points) were recorded with different data sizes, the resolution of neutral loss lines is generally a combination of the resolution in the vertical precursor dimension and of the resolution in the horizontal precursor dimension.

Figure 2h shows the signal for ion species that lose a water molecule in the ICR cell during IRMPD fragmentation. As expected, ions generated from cholesterol as well as in-source fragments such as dehydrogenated species and $[M\text{-}CH_3]^{+\bullet}$ dissociate with water loss (see Figure 2c). The neutral loss scan of 18 Da also shows fragment peaks at *m/z* 385, 386, and 387. The corresponding precursor ion peaks are at *m/z* 403, 404, and 405. The peak at *m/z* 385 can be assigned to $C_{27}H_{47}O_2^+$ (see Table 1 in the Supplementary Materials). The only corresponding precursor ion to the fragment at *m/z* 386 is $^{13}C^{12}C_{26}H_{47}O_2^+$. Since this peak is more intense than the one at *m/z* 385, a large part of the signal intensity can be said to result from the scintillation noise from the signal of the $M^{+\bullet}$ ion from cholesterol. By the same reasoning, the peak at *m/z* 387 can be said to result largely from scintillation noise from the signal resulting from the MH^+ ion of cholesterol. Compounds such as $C_{21}H_{43}O_4^+$, $C_{27}H_{47}O_2^+$, $C_{27}H_{45}O_3^+$, and $C_{28}H_{49}O_3^+$ (see Table 1 in the Supplementary Materials) also dissociate via water loss and thus show peaks in the neutral loss scan of 18 Da. This fragmentation pattern is similar to the ones reported by Rossmann et al. [48], Lembcke et al. [49], and Ronsein et al. [50] for cholesterol oxidations products. Although the product information provided by Sigma Aldrich specifies 99% purity [51] and the extraction and assay of cholesterol follows a well-known protocol [52], the sample was purchased and first opened in 2010, and so partial oxidation may have taken place since this time. As Kauppila et al. have shown, these oxidation products can also arise during ionization in the APPI source [22].

Figure 2i shows the neutral loss scan of 54 Da, corresponding to a loss of C_3H_4N, which is impossible for cholesterol. The solvents of the cholesterol sample in this study are water and acetonitrile. Marotta et al. [18, 53] have shown that in APPI with a krypton lamp, acetonitrile isomerizes and transfers a proton to the analyte molecules, but can also react with another acetonitrile ion or water before reacting with the analyte molecules. This mechanism explains the presence of the peaks in the mass spectrum of cholesterol that have been identified as nitrogenated species (see Figure 1a and Supplementary Information Table S1). C_3H_4N is a species that is generated by acetonitrile. The fact that various species in the 2D mass spectrum lose C_3H_4N by IRMPD indicates that they were formed by a reaction between cholesterol and a reactant species generated by acetonitrile. Peaks corresponding to loss of 39 Da (corresponding to C_2HN), 40 Da (corresponding to C_2H_2N), and 41 Da (corresponding to C_2H_3N), also with precursor *m/z* ratios corresponding to nitrogenated species, corroborate this hypothesis. These contaminant peaks are not particularly intense and would have been missed in a normal MS/MS experiment. But the fragment ion data are already present in the 2D mass spectrum, allowing a subsequent detailed interrogation without rerunning the sample.

Conclusion

In this implementation of 2D APPI FT-ICR mass spectrometry, the 2D data of cholesterol allowed correlation of fragment ions with their radical ion and protonated ion precursors, without the need for multiple MS/MS experiments. The horizontal fragment ion scans and vertical precursor ion scans yielded accurate information on the fragmentation pathways of cholesterol. 2D FT-ICR MS is a data-independent method and a 2D mass

spectrum correlates the fragment ions with their precursor ions, provides information about the order of fragmentation pathways, and can be used to differentiate between dissociation reactions that take place within the ion source or within the ICR cell.

Neutral loss scans, which are parallel to the autocorrelation line but shifted by the mass of the neutral, identify similar ion species undergoing similar fragmentations, which can give further information into their chemical structure. Although the information present in a 2D mass spectrum can be obtained through MS/MS, performing multiple experiments is time-consuming, complex experiments may be required (such as the use of tailored waveforms for sufficiently high resolution within the ICR cell), and additional time and sample would be required for analysis of multiple MS/MS data sets. Furthermore, data visualization with 2D FT-ICR MS is clear and comprehensive, which is not the case for currently existing data visualization software with traditional MS/MS methods. Finally, the data-independent nature of 2D FT-ICR MS insures that structural information is obtained even on ions that are not deemed of interest at the time of the experiment, but which can nevertheless reveal relevant chemical information on the content of the sample or ionization processes.

Although at present the resolution and mass accuracy of 2D FT-ICR MS are not sufficient to determine the molecular formulas of compounds without the help of additional 1D high resolution mass spectra, the primary limitation to do so is computational capacity, which is a problem that can be overcome. Data processing techniques adapted from NMR can also improve the resolution of 2D FT-ICR MS without increasing the size of the datasets and the length of the experiments, such as partial sampling techniques [54, 55].

This study has shown that 2D FT-ICR mass spectrometry is well-adapted to the structural analysis of samples containing small molecules, such as pharmaceuticals, metabolites, or natural products. 2D FT-ICR MS can also be adapted to other fragmentation methods for small molecules, such as electron-induced dissociation (EID) [56, 57].

Acknowledgments

The authors gratefully acknowledge funding for this project by grant no. EP/J000302 from the Engineering and Physical Sciences Research Council. They thank Mr. Jason Noone for his help with computational problems, as well as Dr. Andrea Clavijo-Lopez and Mrs. Ngan Kim Dam for helpful conversations.

References

1. Marshall, A.G., Hendrickson, C.L., Jackson, G.S.: Fourier transform ion cyclotron resonance mass spectrometry: a primer. Mass Spectrom. Rev. **17**, 1–35 (1998)
2. Marshall, A.G., Verdun, F.R.: Fourier transforms in NMR, optical, and mass spectrometry. A user's handbook. Elsevier, Amsterdam (1990)
3. Marshall, A.G., Blakney, G.T., Beu, S.C., Hendrickson, C.L., McKenna, A.M., Purcell, J.M., Rodgers, R.P., Xian, F.: Petroleomics: a test bed for ultra-high-resolution fourier transform ion cyclotron resonance mass spectrometry. Eur. J. Mass Spectrom. **16**, 367–371 (2010)
4. Pfaendler, P., Bodenhausen, G., Rapin, J., Houriet, R., Gäumann, T.: Two-dimensional Fourier transform ion cyclotron resonance mass spectrometry. Chem. Phys. Lett. **138**, 195–200 (1987)
5. Marshall, A.G., Wang, T.C.L., Ricca, T.L.: Ion cyclotron resonance excitation/deexcitation: a basis for stochastic Fourier transform ion cyclotron mass spectrometry. Chem. Phys. Lett. **105**, 233–236 (1984)
6. Guan, S., Jones, P.R.: A theory for two-dimensional Fourier-transform ion cyclotron resonance mass spectrometry. J. Chem. Phys. **91**, 5291–5295 (1989)
7. van Agthoven, M.A., Delsuc, M.-A., Bodenhausen, G., Rolando, C.: Towards analytically useful two-dimensional Fourier transform ion cyclotron resonance mass spectrometry. Anal. Bioanal. Chem. **405**, 51–61 (2013)
8. Pfaendler, P., Bodenhausen, G., Rapin, J., Walser, M.E., Gäumann, T.: Broad-band two-dimensional Fourier transform ion cyclotron resonance. J. Am. Chem. Soc. **110**, 5625–5628 (1988)
9. Bensimon, M., Zhao, G., Gäumann, T.: A method to generate phase continuity in two-dimensional Fourier transform ion cyclotron resonance mass spectrometry. Chem. Phys. Lett. **157**, 97–100 (1989)
10. Ross III, C.W., Guan, S., Grosshans, P.B., Ricca, T.L., Marshall, A.G.: Two-dimensional Fourier transform ion cyclotron resonance mass spectrometry/mass spectrometry with stored-waveform ion radius modulation. J. Am. Chem. Soc. **115**, 7854–7861 (1993)
11. Ross, C., Simonsick Jr., W.J., Aaserud, D.J.: Application of stored waveform ion modulation 2D-FTICR MS/MS to the analysis of complex mixtures. Anal. Chem. **74**, 4625–4633 (2002)
12. van der Rest, G., Marshall, A.G.: Noise analysis for 2D tandem Fourier transform ion cyclotron resonance mass spectrometry. Int. J. Mass Spectrom. **210/211**, 101–111 (2001)
13. van Agthoven, M.A., Delsuc, M.-A., Rolando, C.: Two-dimensional FT-ICR/MS with IRMPD as fragmentation mode. Int. J. Mass Spectrom. **306**, 196–203 (2011)
14. van Agthoven, M.A., Chiron, L., Coutouly, M.-A., Delsuc, M.-A., Rolando, C.: Two-dimensional ECD FT-ICR mass spectrometry of peptides and glycopeptides. Anal. Chem. **84**, 5589–5595 (2012)
15. van Agthoven, M.A., Coutouly, M.-A., Rolando, C., Delsuc, M.-A.: Two-dimensional Fourier transform ion cyclotron resonance mass spectrometry: reduction of scintillation noise using Cadzow data processing. Rapid Commun. Mass Spectrom. **25**, 1609–1616 (2011)
16. Chiron, L., van Agthoven, M.A., Kieffer, B., Rolando, C., Delsuc, M.-A.: Efficient denoising algorithms for large experimental datasets and their applications in Fourier transform ion cyclotron resonance mass spectrometry. Proc. Natl. Acad. Sci. U. S. A. **111**, 1385–1390 (2014)
17. van Agthoven, M.A., Chiron, L., Coutouly, M.-A., Sehgal, A.A., Pelupessy, P., Delsuc, M.-A., Rolando, C.: Optimization of the discrete pulse sequence for two-dimensional FT-ICR mass spectrometry using infrared multiphoton dissociation. Int. J. Mass Spectrom. **370**, 114–124 (2014)
18. Raffaelli, A., Saba, A.: Atmospheric pressure photoionization mass spectrometry. Mass Spectrom. Rev. **22**, 318–331 (2003)
19. Robb, D.B., Covey, T.R., Bruins, A.P.: Atmospheric pressure photoionization: an ionization method for liquid chromatography-mass spectrometry. Anal. Chem. **72**, 3653–3659 (2000)
20. Barrow, M.P., Witt, M., Headley, J.V., Peru, K.M.: Athabasca oil sands process water: characterization by atmospheric pressure photoionization and electrospray ionization Fourier transform ion cyclotron resonance mass spectrometry. Anal. Chem. **82**, 3727–3735 (2010)
21. Griffiths, M.T., Da Campo, R., O'Connor, P.B., Barrow, M.P.: Throwing light on petroleum: simulated exposure of crude oil to sunlight and characterization using atmospheric pressure photoionization fourier transform ion cyclotron resonance mass spectrometry. Anal. Chem. **86**, 527–534 (2014)
22. Kauppila, T.J., Kuuranne, T., Meurer, E.C., Eberlin, M.N., Kotiaho, T., Kostiainen, R.: Atmospheric pressure photoionization mass spectrometry. Ionization mechanism and the effect of solvent on the ionization of naphthalenes. Anal. Chem. **74**, 5470–5479 (2002)
23. Wyllie, S.G., Amos, B.A., Tokes, L.: Electron impact induced fragmentation of cholesterol and related C-5 unsaturated steroids. J. Org. Chem. **42**, 725–732 (1977)
24. Gabrielse, G., Haarsma, L., Rolston, S.L.: Open-endcap Penning traps for high precision experiments. Int. J. Mass Spectrom. Ion Processes **88**, 319–332 (1989)
25. Kilgour, D.P.A., Wills, R., Qi, Y., O'Connor, P.B.: Autophaser: an algorithm for automated generation of absorption mode spectra for FT-ICR MS. Anal. Chem. **85**, 3903–3911 (2013)

26. Qi, Y., Barrow, M.P., Van Orden, S.L., Thompson, C.J., Li, H., Perez-Hurtado, P., O'Connor, P.B.: Variation of the Fourier transform mass spectra phase function with experimental parameters. Anal. Chem. **83**, 8477–8483 (2011)
27. Qi, Y., Barrow, M.P., Li, H., Meier, J.E., Van Orden, S.L., Thompson, C.J., O'Connor, P.B.: Absorption-mode: the next generation of fourier transform mass spectra. Anal. Chem. **84**, 2923–2929 (2012)
28. Qi, Y., Li, H., Wills, R.H., Perez-Hurtado, P., Yu, X., Kilgour, D.P.A., Barrow, M.P., Lin, C., O'Connor, P.B.: Absorption-mode Fourier transform mass spectrometry: the effects of apodization and phasing on modified protein spectra. J. Am. Soc. Mass Spectrom. **24**, 828–834 (2013)
29. Qi, Y., Thompson, C.J., Van Orden, S.L., O'Connor, P.B.: Phase correction of Fourier transform ion cyclotron resonance mass spectra using MatLab. J. Am. Soc. Mass Spectrom. **22**, 138–147 (2011)
30. Qi, Y., Witt, M., Jertz, R., Baykut, G., Barrow, M.P., Nikolaev, E.N., O'Connor, P.B.: Absorption-mode spectra on the dynamically harmonized Fourier transform ion cyclotron resonance cell. Rapid Commun. Mass Spectrom. **26**, 2021–2026 (2012)
31. Qi, Y., O'Connor, P.B.: Data processing in Fourier transform ion cyclotron resonance mass spectrometry. Mass Spectrom. Rev. **33**, 333–352 (2014)
32. Cho, Y., Qi, Y., O'Connor, P.B., Barrow, M.P., Kim, S.: Application of phase correction to improve the interpretation of crude oil spectra obtained using 7 T Fourier transform ion cyclotron resonance mass spectrometry. J. Am. Soc. Mass Spectrom. **25**, 154–157 (2014)
33. Ledford Jr., E.B., Rempel, D.L., Gross, M.L.: Space charge effects in Fourier transform mass spectrometry. II. Mass calibration. Anal. Chem. **56**, 2744–2748 (1984)
34. Pons, J.-L., Malliavin, T.E., Delsuc, M.A., Gifa, V.: 4: a complete package for NMR data set processing. J. Biomol. NMR **8**, 445–452 (1996)
35. Francl, T.J., Sherman, M.G., Hunter, R.L., Locke, M.J., Bowers, W.D., McIver Jr., R.T.: Experimental determination of the effects of space charge on ion cyclotron resonance frequencies. Int. J. Mass Spectrom. Ion Processes **54**, 189–199 (1983)
36. Shi, S.D.H., Drader, J.J., Freitas, M.A., Hendrickson, C.L., Marshall, A.G.: Comparison and interconversion of the two most common frequency-to-mass calibration functions for fourier transform ion cyclotron resonance mass spectrometry. Int. J. Mass Spectrom. **195/196**, 591–598 (2000)
37. Chapman, J.D., Goodlett, D.R., Masselon, C.D.: Multiplexed and data-independent tandem mass spectrometry for global proteome profiling. Mass Spectrom. Rev. **33**, 452–470 (2014)
38. Louris, J.N., Brodbelt-Lustig, J.S., Cooks, R.G., Glish, G.L., Van Berkel, G.J., McLuckey, S.A.: Ion isolation and sequential stages of mass spectrometry in a quadrupole ion trap mass spectrometer. Int. J. Mass Spectrom. Ion Processes **96**, 117–137 (1990)
39. Chen, L., Wang, T.C.L., Ricca, T.L., Marshall, A.G.: Phase-modulated stored waveform inverse Fourier transform excitation for trapped ion mass spectrometry. Anal. Chem. **59**, 449–454 (1987)
40. O'Connor, P.B., McLafferty, F.W.: High-resolution ion isolation with the ion cyclotron resonance capacitively coupled open cell. J. Am. Soc. Mass Spectrom. **6**, 533–535 (1995)
41. de Koning, L.J., Nibbering, N.M.M., van Orden, S.L., Laukien, F.H.: Mass selection of ions in a Fourier transform ion cyclotron resonance trap using correlated harmonic excitation fields (CHEF). Int. J. Mass Spectrom. Ion Processes **165/166**, 209–219 (1997)
42. McDonald, L.A., Barbieri, L.R., Carter, G.T., Kruppa, G., Feng, X., Lotvin, J.A., Siegel, M.M.: FTMS structure elucidation of natural products: application to muraymycin antibiotics using ESI multi-CHEF SORI-CID FTMSn, the top-down/bottom-up approach, and HPLC ESI capillary-skimmer CID FTMS. Anal. Chem. **75**, 2730–2739 (2003)
43. Wills, R.H., O'Connor, P.B.: Structural characterization of actinomycin d using multiple ion isolation and electron induced dissociation. J. Am. Soc. Mass Spectrom. **25**, 186–195 (2014)
44. Wang, T.C.L., Ricca, T.L., Marshall, A.G.: Extension of dynamic range in Fourier transform ion cyclotron resonance mass spectrometry via stored waveform inverse Fourier transform excitation. Anal. Chem. **58**, 2935–2938 (1986)
45. Guan, S., Marshall, A.G.: Stored waveform inverse Fourier transform (SWIFT) ion excitation in trapped-ion mass spectrometry: theory and applications. Int. J. Mass Spectrom. Ion Processes **157/158**, 5–37 (1996)
46. Julian Jr., R.K., Cooks, R.G.: Broad-band excitation in the quadrupole ion trap mass spectrometer using shaped pulses created with the inverse Fourier transform. Anal. Chem. **65**, 1827–1833 (1993)
47. Budzikiewicz, H., Ockels, W.: Mass spectrometric fragmentation reactions. VIII. Characteristic fragments of 5-unsaturated 3-hydroxysteroids. Tetrahedron **32**, 143–146 (1976)
48. Rossmann, B., Thurner, K., Luf, W.: MS-MS fragmentation patterns of cholesterol oxidation products. Monatsh. Chem. **138**, 437–444 (2007)
49. Lembcke, J., Ceglarek, U., Fiedler, G.M., Baumann, S., Leichtle, A., Thiery, J.: Rapid quantification of free and esterified phytosterols in human serum using APPI-LC-MS/MS. J. Lipid Res. **46**, 21–26 (2005)
50. Ronsein, G.E., Prado, F.M., Mansano, F.V., Oliveira, M.C.B., Medeiros, M.H.G., Miyamoto, S., Di Mascio, P.: Detection and characterization of cholesterol-oxidized products using HPLC coupled to dopant assisted atmospheric pressure photoionization tandem mass spectrometry. Anal. Chem. **82**, 7293–7301 (2010)
51. Available at: http://www.sigmaaldrich.com/content/dam/sigma-aldrich/docs/Sigma/Product_Information_Sheet/c8667pis.pdf. Accessed 12 Jul 2015
52. Stadtman, T.C.: Preparation and assay of cholesterol and ergosterol. Methods Enzymol. **3**, 392–394 (1957)
53. Marotta, E., Seraglia, R., Fabris, F., Traldi, P.: Atmospheric pressure photoionization mechanisms 1. The case of acetonitrile. Int. J. Mass Spectrom. **228**, 841–849 (2003)
54. Delsuc, M.A., Lallemand, J.Y.: Improvement of dynamic range in NMR by oversampling. J. Magn. Reson. **69**, 504–507 (1986)
55. Delsuc, M.-A., Tramesel, D.: Application of maximum-entropy processing to NMR multidimensional data sets: partial sampling case. C. R. Chim. **9**, 364–373 (2006)
56. Wei, J., Li, H., Barrow, M.P., O'Connor, P.B.: Structural characterization of chlorophyll-a by high resolution tandem mass spectrometry. J. Am. Soc. Mass Spectrom. **24**, 753–760 (2013)
57. Mosely, J.A., Smith, M.J.P., Prakash, A.S., Sims, M., Bristow, A.W.T.: Electron-induced dissociation of singly charged organic cations as a tool for structural characterization of pharmaceutical type molecules. Anal. Chem. **83**, 4068–4075 (2011)